Coupled in-situ electrical and optical characterization to assess the accelerated ageing of perovskite solar cells

Alexandra Levtchenko, Arthur Julien, Daniel Mcdermott, Jean-baptiste Puel, Jean-françois Guillemoles, Daniel Ory, Daniel Suchet

Coupled in-situ electrical and optical characterization to assess the accelerated ageing of perovskite solar cells

A. Levtchenko[1], A. Julien[1,2], D. McDermott[2], J.-B. Puel[3], J.-F. Guillemoles[2], D. Ory[3] and D. Suchet[2]

[1] Institut Photovoltaïque d'Ile-de-France (IPVF), 18 Boulevard Thomas Gobert, 91120 PALAISEAU, France
e-mail: alexandra.levtchenko@ipvf.fr
[2] Institut Photovoltaïque d'Ile-de-France (IPVF), UMR 9006, CNRS, École Polytechnique - IP Paris, Chimie Paris-Tech PSL, Palaiseau, 91120, France
[3] EDF R&D, France

the date of receipt and acceptance should be inserted later

Abstract. While perovskite-based solar cells exhibit excellent efficiencies and require a relatively simple synthesis process, stability issues during operation severely limit their commercial development. Therefore, degradation studies have drawn much attention, but the plethoric literature highlights the complexity of the topic. Thus far, most studies perform pre- and post-mortem analysis and compare the system's performance before and after aging, severely limiting the understanding of degradation pathways. By contrast, *in-situ* characterization allows the degradation to be tracked in real time and the pathways to be fully explored. To this end, a coupled IV-photoluminescence (PL) characterization bench has been set up inside a climate chamber, allowing for the periodic acquisition of PL spectra and IV curves during accelerated aging. In this study, the ISOS protocol damp heat test (65°C, 85% RH) was applied to several perovskite solar cells with various transport layer combinations. By following the evolution kinetics of PL spectra and IV curves, insights into the nature of the degradation mechanisms are obtained. Notably, it becomes possible to distinguish performance losses due to degradation of the perovskite absorber from those where extracting layers are the cause.

Key words. Accelerated aging, reliability, perovskite, solar cells, photovoltaics, in-situ

1 Introduction

In the past decade, perovskite solar cells have been shown to rival the efficiency of standard silicon cells, with power conversion efficiencies as high as 26.7% [1]. However, the main barrier to upscaling and deployment of these cells remains their stability. While a commercial silicon module can operate for 30 years with limited performance loss, perovskite cells are subject to a variety of degradation processes [2–5]. Furthermore, the driving mechanisms degrading a solar cell depend not only on the specific composition of the perovskite itself but also on the device architecture, the encapsulation, and the combination of environmental factors (notably light, heat, bias, and moisture) [3, 4, 6, 7]. The community is making efforts to assess the stability of perovskite solar cells under accelerated aging [8, 9]. While ion migration and trapped charges were identified as responsible for perovskite degradation [10], the hole transporting layer, interface passivation, and buffer layers are also known to be prone to degradation [11–13].

Characterizing and investigating the aging of a perovskite solar cell is therefore a complex yet critical task that requires careful observation.

Among the broad variety of characterization techniques, two appear particularly well suited for a complementary analysis of the opto-electronic degradation of perovskite solar cells. Current-voltage (IV) measurements under illumination allow a direct estimation of the device's ultimate objective, i.e. power conversion efficiency (PCE), together with key performance indicators such as the open-circuit voltage (V_{OC}), short-circuit current density (J_{SC}), and fill factor (FF). Comparing IV characteristics both in the dark and under illumination can also shed light on the device's collection efficiency. However, IV indicators are aggregated quantities, and their evolution can be indiscriminately attributed to several internal processes. To lift this ambiguity, it can be useful to complement IV measurements with photoluminescence (PL) spectroscopy, which unveils the optical properties of the materials. and will notably allow both variations in the sample structure and the formation of trap states to be estimated. Perovskite samples are particularly well suited for PL analysis owing to their excellent radiative properties.

These two techniques are routinely used to characterize perovskite samples. However, from the perspective of aging tests, it may not be sufficient to perform these analyses at the beginning and at the end of the test. Tracking

the evolution of the opto-electronic performances *in-situ* is crucial to estimate the degradation dynamics, and in turn the mechanisms at stake [14,15]. Such an *in-situ* analysis is even more critical for accelerated aging tests, where the dynamics of degradation can serve as a signature to relate the artificial conditions to real-world situations [16].

Both IV [6,17] and PL [3,4,18–20] have already been successfully used for *in-situ* aging tests, but only independently. In this work, the development of an experimental set-up allowing simultaneous IV and PL measurements inside a climate chamber operating the accelerated aging of perovskite solar cells is reported. We show that the combination of the two techniques helps to distinguish if the major degradation mechanism comes from the deterioration of the active layer or extraction/collection properties. Then, by combining experimental results with numerical methods, we explore ways to gain more insight into the origins of the degradation. Namely, shunt pathways can be identified and qualified by fitting the IV curves, while degradation modeling effectively helps to rule out some of the possible degradation mechanisms.

2 Methods

2.1 Sample fabrication

Solar cells fabrication Two different samples have been investigated in this work (see table 1).

Both samples have a similar n-i-p structure. The bottom electrode is patterned by laser scribing (InnoLas) on FTO-coated 3mm glass substrates (TEC10, Solems). The surface is cleaned by a tree-step sonification process by successive bath of RBS concentrate at 2% in water (Sigma Aldrish), Aceton and Isopropanol (Mon Droguiste, >99.5%).

Compact titanium dioxide (TiO_2) layer (15 nm) is grown by atomic layer deposition (ALD) as described in [21] and a mesoporous TiO_2 is added (100 nm) by spin-coating (1:7 weight ratio of TiO_2 paste solution in Ethanol anhydrous denaturated, Sigma Aldrish, 90%, speed : 4000 rpm, duration : 30s). The substrate was immediately annealed on a hot plate for 45 min with several temperature steps, up to 500°C. After cool-down the TiO_2-coated substrates are treated with UV-Ozone for 30 min before being introduced under inert nitrogen atmosphere in a glovebox for perovskite and HTL deposition. An alternative ETL is made of 10 nm tin oxide (SnO_2) grown by ALD [22], then completed by 50 nm of SnO_2 deposited by Chemical Bath Deposition (CBD) at 90°C [23] and treated with 0,15mM potassium chloride (KCl, Sigma Aldrish ¿ 99%). The absorber is a triple cation perovskite (400 nm) prepared by mixing PbI_2 and $PbBr_2$ (ultra dry 99.999%, Alfa Aesar), FAI and MABr (>99.99%, Greatcell Solar Materials), and CsI(99.999%, Sigma-Aldrich) in DMF (anhydrous 99.8 %, Sigma-Aldrich):DMSO (>99.7%, Sigma-Aldrich) (4:1; v:v) and deposited by spin-coating (speed: 2000 rpm, duration: 12s, a second consecutive step of 30 s at 6000 rpm was used to deposit 100 μL of chlorobenzene 12s before the end of the rotation). The obtained $Cs_{0,05}(MA_{0,167}FA_{0,833})_{0,95}Pb(I_0,842Br_{0,158})_3$ perovskite-coated substrate was immediately annealed at 100°C for 30 min. The hole transport layer (HTL) is composed of a 20 nm thick spin-coated polytriarylamine solution composed of 10 mg of PTAA (Solaris Chemical), 3.75 μl of tBP (Sigma-Aldrich, 98%), 2.4 μl of Li-TFSi (Sigma-Aldrich, 99.95%), per 1 ml of toluene (Sigma-Aldrich, 99.8%) 3000 rpm, 30s.

To complete the stack, a gold back contact (100 nm) was thermally evaporated under high vacuum conditions through a shadow mask to define the active area.

In sample 2, the perovskite contains a Lead(II) thiocyanate (sigma Aldrich, 99.5%) $Pb(SCN)_2$ additive of 1% in concentration.

Encapsulation process The devices are encapsulated in a Glass/Glass configuration using Polyisobutylene (PIB) as an edge sealant. The lamination process is performed at 120°C for 16 min.

2.2 Experimental measurements

We developed an experimental setup coupling photoluminescence (PL) and current-voltage (IV) characterization techniques (Figure 1) that we place inside of a climate chamber (SunEvent, Weisstechnik).

The PL setup consists of a light source (660 nm laser beam (gem, Laser Quantum)) and a spectrometer (AvaSpec ULS TEC EVO, Avantes), both fibered to access the chamber. Collimation optics are inserted inside the chamber and experience the same conditions as the sample; we check on a regular basis that the properties of the optics remain unaffected. The illumination intensity is approximately 25 mW/cm^2, thus respecting low injection conditions.

The IV measurement is performed thanks to a precision source/measure unit (B2911A, Keysight) connected to the busbars of the sample by electrical cables and alligator clips. The voltage scan can either be performed up to a fixed voltage (1.2 V for sample 1) or stop once the open circuit voltage is reached (sample 2). Both forward and reverse scans have been performed, with a scanning rate of 20 mV/s. The two samples showed limited hysteresis, and we focused on the indicators obtained over forward scans in the following.

The measurements are automated with LabVIEW software and allow the cycle depicted in Figure 2 to be performed repeatedly. The frequency of the acquisitions is set by the user. In this case, each cycle lasts 20 minutes, with 5 minutes of acquisition time and 15 minutes of waiting time before the next acquisition. During the acquisition time, the following measurements are performed: PL, light IV under laser illumination, and dark IV (laser off). The laser source is switched off during the waiting time, e.g. in between each acquisition, to reduce the disturbance of the samples by the measurement system.

It is possible that the optical and electrical stimulation affects the aging of the sample. In general, it would

Table 1. Characteristics of the devices aged under constant conditions (85% R.H., 65°C, dark) in a climatic chamber and periodically characterized through JV and PL measurements. Composition of the triple-cation perovskite (3C-PVK): $Cs_{0,05}(MA_{0,167}FA_{0,833})_{0,95}Pb(I_0,842Br_{0,158})_3$.

Sample	1	2
ETL	Glass / FTO / SnO_2	Glass / FTO / TiO_2
Absorber	3C - PVK	3C - PVK +1%$Pb(SCN)_2$
HTL	PTAA / Au	PTAA / Au
Voltage scan	0 - 1.2 V	0 - V_{oc}

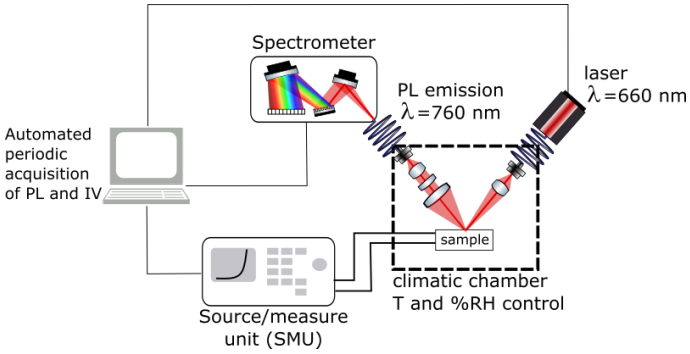

Fig. 1. Schematic view of the experimental setup

be important to compare the monitored sample at the end of the aging process with an unmonitored sample to check whether their final states are identical. The results presented in this work aim at providing a proof of concept of the analysis technique, not at investigating a specific degradation mechanism, and this verification will thus be omitted.

2.3 Accelerated aging

The aging imposed on the samples is close to the ISOS-D-3 protocol from the consensus statement for stability assessment and reporting for perovskite photovoltaics [7]. It consists in placing the sample in an environmental chamber with 85 %RH and 65 °C (or 85 °C). In between the measurements, the samples are left in the dark. The light source for the device performance characterization should be a solar simulator; however, in this study, we chose to operate with the laser as the light source for in-situ IV, so they are directly comparable to the PL measurements.

2.4 Models

Generalized Planck's law The PL measurements performed in this work have been analyzed by referring to the generalized Planck law, as it relates the spectral distribution of the signal with the absorptivity of the sample, $A(h\nu)$, and the quasi-Fermi levels splitting (qFls), $\Delta\mu$:

$$I_{PL}(h\nu) = A(h\nu)\frac{(h\nu)^2}{4\pi^2\hbar^3c^2}\frac{1}{\exp\left(\frac{h\nu-\Delta\mu}{k_BT}\right)-1} \qquad (1)$$

where $\hbar$ is the reduced Planck constant and c the speed of light [24,25].

As reported below, the absorptivity $A(h\nu)$ of all studied samples remains almost unchanged after the first few hours of aging. This allows us to estimate the time evolution of the quasi-Fermi level splitting ($\Delta\mu$) within the absorber as:

$$\Delta\mu(t_1) - \Delta\mu(t_0) \simeq k_BT \ln\frac{\int d(h\nu)\, I_{t_1}(h\nu)}{\int d(h\nu)\, I_{t_0}(h\nu)} \qquad (2)$$

Drift diffusion simulations In order to analyze the aging measurements exposed above, a specific modeling scheme has been developed. It is based on coupled optical (transfer matrices with in-house code) and electrical (drift-diffusion with SCAPS-1D [26]) modeling. The approach is explained in detail in [16], and the specifics of simulating a photoluminescence spectrum are available in the supplementary material. It allows the initial performances of the devices to be reproduced and, more specifically, their response to several degradation mechanisms to be simulated. For instance, the response to a formation of defects in the perovskite layer, a reduction of electron mobility in the ETL, and the formation of defects at the perovskite-HTL interface will be investigated.

The distinction of degradation mechanisms is obtained by comparing experimental and simulated results. Instead of focusing on the evolution of the solar cell's opto-electronic parameters (such as V_{OC} and J_{SC}) throughout the aging process, it is useful to consider their correlations. The evolution of such correlations describes pathways in the V_{OC}-J_{SC} plane, for instance. They are independent from time and any speed of reaction, and therefore from any activation process through environmental conditions such as temperature or irradiance. The degradation pathways are intrinsic characteristics of the processes responsible for the observed degradation, allowing simulations to be compared to experiments.

Current-voltage model To investigate the origin of the degradation occurring, we fitted dark JVs curves using the 2/3-diode fit software developed by Suckow [27]. Our method for establishing the model was to define its characteristics in such a way as to make it as simple as possible, i.e. with as few floating parameters as possible, and usable for all the IV curves throughout the aging process.

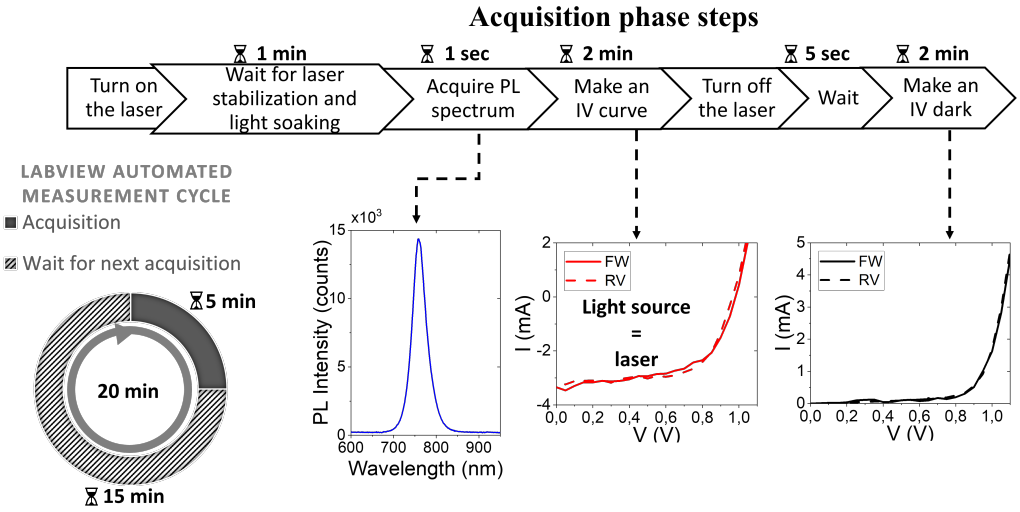

Fig. 2. Measurement cycle diagram

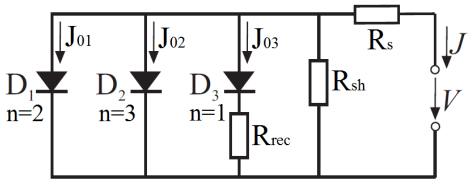

Fig. 3. Equivalent electrical model used for fitting the dark JV data. It includes a third diode in parallel with the others and associated with a resistance in series, R_{rec}. This resistance limits the current flowing through the 3rd diode.

We started from a one-diode model with all parameters floating, and step by step, we had to introduce a second and afterwards a third diode in series with a resistance $R_{\rm rec}$ [28,29]. The latter has been introduced in the literature to account for surface damage. A large initial value of $R_{\rm rec}$ prevents the current from flowing in this branch, and the third diode has no influence on the IV curve, but as the system degrades, $R_{\rm rec}$ decreases and the influence of the third diode increases.

It turned out that the three ideality factors did not vary significantly with time, and we chose to fix them at the nearest integer value, leaving only the resistors and dark currents adjustable. Consequently, the electrical model defines the recombination pathways involved, and their respective evolution during aging is described by the floating parameters. The electrical model is presented in Fig. 3 for sample 1.

3 Results

IV curves and PL spectra were collected during the accelerated aging according to the cycle diagram depicted in Figure 2. Figure 4 shows their evolution for the two investigated samples. We emphasize that the illumination for IV measurements is performed by a monochromatic laser source, which does not follow a standard AM1.5 spectrum. Therefore, the results reported here should not be compared to values obtained in a solar simulator but can be used to estimate the relative evolution of the devices' performances.

The figures of merit, such as $V_{\rm OC}$, $J_{\rm SC}$, FF, and total PL emission, are shown throughout the full aging experiment in SI, Figures S1 and S2. Both optical and electrical indicators show an initial transient behavior, with a slight improvement of the performances. This behavior takes place over the first 10 to 50 hours and is followed by a steady degradation of the photovoltaic performance over the remaining duration of the experiment. In this study, we focus on the long-term steady evolution associated with a decrease in performances. In Figures S1 and S2, the corresponding data is depicted with red crosses.

Time sequences of Figure 4 correspond to this specific regime. We see that the degradation is particularly severe for sample 1, with a very strong loss of $V_{\rm OC}$. Taken alone, this effect could be interpreted as the degradation of the absorber material. However, the spectral shape of the luminescence emission remains remarkably unchanged throughout the aging test. In particular, we notice no evolution of the optical bandgap and no broadening of the low energy tail. This rules out a significant chemical alteration of the absorber and justifies our application of eq. 2 to estimate the time evolution of the internal voltage.

The complementarity of PL and IV measurements is especially striking when comparing the evolution of the internal voltage, estimated as the qFls, and the open circuit voltage $V_{\rm OC}$ (Fig. 5). Focusing on the investigated sequences, the $V_{\rm OC}$ drop could be attributed to a degradation of the perovskite material itself, which seems not to be the case as the internal voltage remains stable for both samples. Therefore, the voltage loss is probably caused by degradation of extraction/transport layers and/or contacts. This decoupling of the internal and external voltage is particularly dramatic for sample 1.

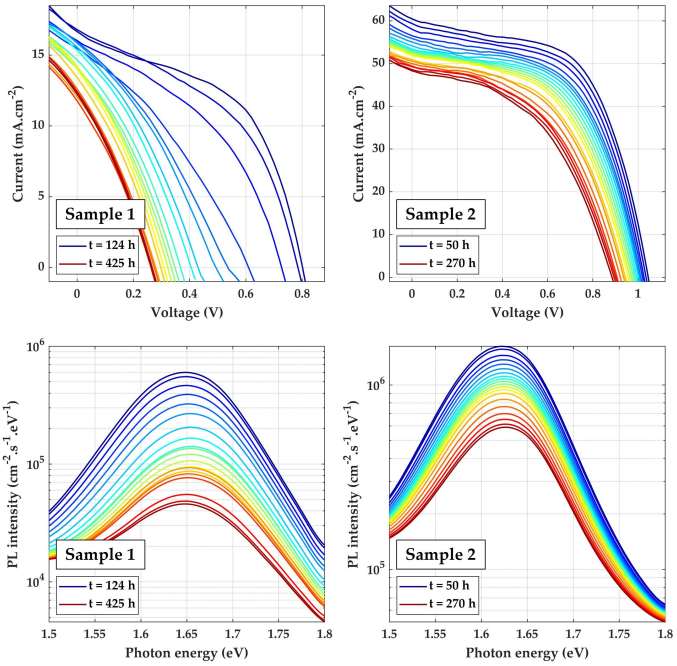

Fig. 4. Evolution of JV curves and PL spectra during investigated aging sequences for the three samples aged at 65°C and 85 % RH.

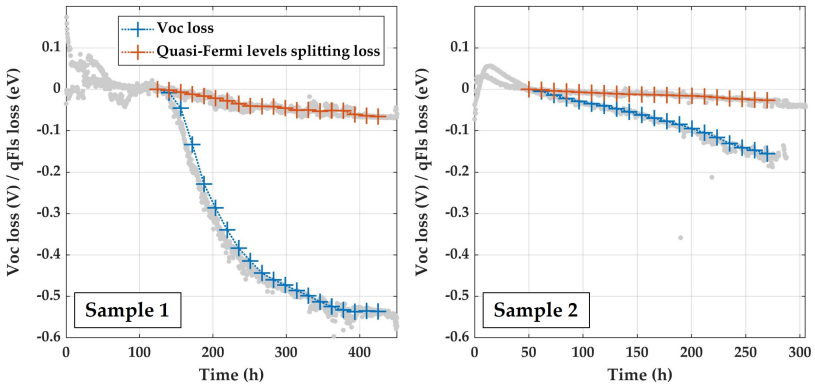

Fig. 5. Loss of V_{oc} and quasi-Fermi levels splitting over time, during investigated time sequences.

Complementary experiments performed on an inverted p-i-n structure with inorganic CTL (NiO_x and SnO_2, respectively) and a silver top electrode don't show the degradation reported before (see supplementary material, Fig. S3). Consequently, we believe that the observed V_{oc} reduction is the result of organic PTAA degradation and/or gold migration from the contact, and we will discuss these possibilities.

4 Discussion

4.1 Analysis of the IV curves

Here we first discuss the results of fitting the dark IV curves recorded for sample 1 using the 3-diode model presented previously. The ideality factor for the first diode is set to $n_1 = 2$, which notably corresponds to defect-induced recombination in intrinsic regions. The ideality factor of the second diode is set to $n_2 = 3$, a phenomenological value that has been associated with several surface-induced recombinations [30–32]. The third diode has an ideality factor of $n_3 = 1$, which usually corresponds to bimolecular recombination and was also found in literature for HTL-free perovskite solar cells[33].

In Fig. 6 (a) and (b), we depict the time evolution of the electrical parameters estimated from the fits, namely the shunt (R_{sh}) and series (R_s) resistances, as well as the three dark recombination currents associated with the diodes (J_{01}, J_{02}, J_{03}), the third of which also has its own series resistance (R_{rec}). The dramatic decrease of the open circuit voltage between 100 and 200 h observed in Fig. 5 is shown to be accompanied by a decrease by a factor 20 of the shunt resistance. Formation of shunts could

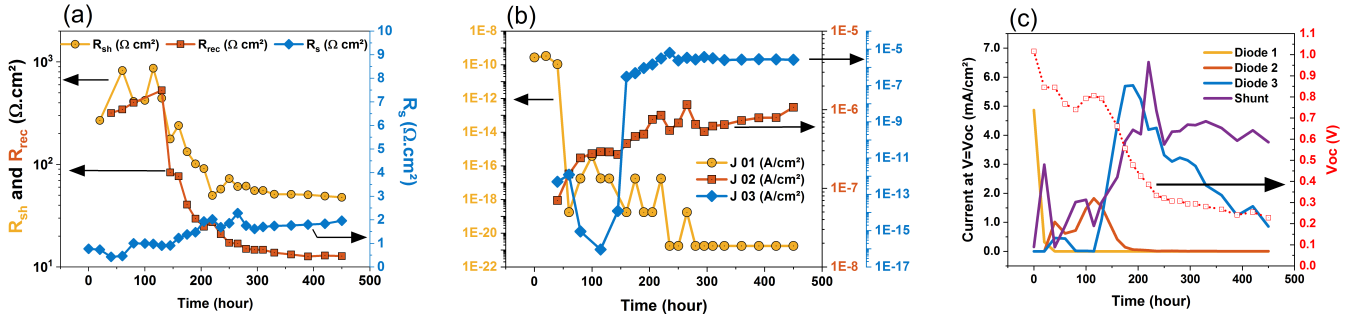

Fig. 6. Time evolution of (a): fitted resistances R_{sh}, R_s and R_{rec}, (b): Dark recombination current J_{01}, J_{02} and J_{03} associated to diodes 1 to 3, (c) currents at V=V_{oc} (right scale in red) flowing through the shunt and the three diodes (left scale). All outliers were removed.

then be suspected to be the main source of degradation. At the same time, the third diode becomes predominant among recombination currents, and we see that the resistance R_{rec} is reduced by almost two orders of magnitude, allowing the current to flow in this branch of the circuit. This demonstrates a change in the current pathway.

After 200h of aging, R_{sh} and R_{rec} stabilize to values as low as 50 and 20 Ω.cm^2 respectively, and the dark current density of diode 3 stays dominant.

Due to the difference of ideality factors and the presence of a series resistance, the relative contribution of each recombination pathway cannot be straightforwardly estimated from the dark currents $J_{0,i}$. Instead, we computed all recombination currents at V_{OC} (obtained from JV measurements under illumination) and plotted them in Fig. 6 (c). V_{OC} is also depicted with red squares and relates to the right vertical axis.

First, it can be noted that at the beginning of the aging, SRH recombination was probably prevailing, as diode 1 (n_1=2) is associated with the largest current. This dominance of SRH recombination over radiative recombination, even for fresh perovskite solar cells, has already been reported in literature [33].

Second, the roles of the third diode and shunt resistance regarding degradation now appear more clearly, as they become the two major loss channels after 150 h. Both reach values above 5 mA.cm^{-2} very rapidly before decreasing. In the long term, losses through the shunt resistance appear to remain dominant as the curve stabilizes at a value of 4 mA.cm^{-2}, whereas the current of the third diode continues to decrease.

Hereafter, we propose an explanation for the observed evolution of the third diode (see Supplementary Information for further details). The evolution over time of the third diode JV, as depicted in Fig. S10, appears to be composed, after a short transition, of a decrease in energy position associated with a rise in intensity.

To challenge this idea, we simulated a simplified SCAPS model [26] to compute the JV characteristics of a pristine cell (Contact, PTAA, Pvk, ETL, Contact) without series nor shunt resistance. The perovskite absorber here is treated as a material with a bandgap E_g=1.6 eV and a deep middle-gap defect with density N_t=$10^{16} cm^{-3}$. Then we simulated the same stack without the PTAA layer to account for its degradation (for example, evaporation of volatile species) and with varying defect properties. We investigated the type of the defect (donor, neutral, acceptor), the defect energy position (donor, N_t=$10^{16} cm^{-3}$), and density (donor, E_c-0.8 eV). These are reported in Figure S10 (a), (b), and (c). We also explore the transition from the pristine cell to a cell without PTAA in Fig. S11 (d) by changing the proportion of the surface of PTAA evaporated or degraded.

This study shows that the qualitative shape of the observed JV curve (Fig. S10) resembles that obtained with a donor impurity (Fig. S11 (a)). We also observe that changing the energetic position or concentration of the defects leads to an homotetic transform (intensity rise and/or energy shift) of the curve (Fig. S11 (b) and (c)). To further corroborate this observation, we compute the second derivatives of the JV curves (Fig. S11) and show that they are simply translated along the voltage axis.

We are then able to assess that by combining the defect type (donor), its energy position, density, and damaged surface ratio, the time evolution of the third diode JV can be reproduced quite well by our modeling. Noticeably, the ideality factors of the JVs of Fig. S11 (b) and (c) are almost equal to n = 1, as we obtained by fitting the experimental JVs.

This joint analysis of IV measurements under dark and illumination provides a clearer picture of the losses at V_{OC}. It relates degradation of the solar cell to a formation of shunts, possibly induced by the removal of the PTAA layer, which translates as a decrease of the shunt resistance and an increased contribution of diode 3 [30, 31]. This possible explanation will be further supported by the joint IV and PL analysis in the following section.

4.2 Joint PL-IV analysis: degradation pathways

Following the method introduced by Julien *et al.* [16], we will now consider the degradation pathways obtained from the experimental results. It consists of representing the evolution of the correlations between opto-electronic parameters, so their positions are time-independent.

In order to investigate and pin down the origin of the degradation, we model the evolution of sample 1 according to the method described in detail in [16].

Using simulation, we first determine 114 sets of input parameters that closely replicate the initial IV and PL performances (see supplementary material, Fig. S4). Then, we degrade some of these parameters, corresponding to 12 possible degradation mechanisms listed in the legend of Fig. 7. They are probable causes of the degradation, given the vast literature reporting numerous instability issues of perovskite solar cells [5]. Each of these mechanisms leads to a specific pathway in the parameter spaces displayed in this figure. Finally, we compare these simulated pathways to the experimental results (black dots).

If a degradation pathway induces a close pathway to the experiment on all planes, it is considered compatible and can be a cause of degradation. This is the case for the decrease of shunt resistance (green triangles): the first experimental points follow the same joint decrease of Jsc and Voc and a strong loss of FF. Also, on the plane showing qFls versus Voc, the major Voc variation is reproduced.

It is worth noting that another simulated mechanism induces a pathway close to the experimental behavior: the formation of defects at the pvk/ETL interface (red triangles). The range of variation for Voc would be underestimated, but pathways remain generally compatible.

On the contrary, all other mechanisms are excluded because of distinct pathways on at least one plane. This is the case, for instance, for the reduction of hole mobility in the perovskite layer (yellow squares). The initial Jsc-Voc trend and significant FF loss are well reproduced; however, this mechanism should induce an increase in PL emission and quasi-Fermi level splitting, while the contrary is observed experimentally.

This example illustrates the advantage of combining JV and PL measurements. If only JV parameters had been available, the decrease in hole mobility would have been a compatible candidate. However, the second measurement provides useful complementary insights.

The degradation of the perovskite layer has also been mentioned previously as a possible cause of a solar cell's V_{OC} loss. Again, the coupled measurements bring insights here: a formation of defects in the absorber (yellow circles) indeed induces similar pathways to experiment in the planes related to IV parameters. However, it leads to too strong a degradation of qFls, where the experiment shows stability. This excludes the possibility for this mechanism to explain the solar cell behavior.

The joint IV-PL analysis presented in this section corroborates the previous results of fitting the dark IV measurements, where it has been exposed that the degradation of sample 1 may be attributed to the formation of shunts. Similarly, simulations show that the degradation of this sample could be linked to both the formation of shunts and surface defects.

Sample 2 has also been investigated with the same approach, with 116 sets of parameters employed to reproduce initial performances (Fig. S4). Obtained degradation pathways are reported in supplementary material (Fig. S5). In this second case, we also found the decrease of shunt resistance to be a compatible mechanism, but reductions of doping in ETL or HTL could also explain the degradation. Similar conclusions were also found for a third sample, which has the same architecture as sample 2 but an additional 2D-PEAI passivation between the perovskite layer and the HTL and no $Pb(SCN)_2$ additive in the perovskite [34]. The results for this sample are depicted in Figs. S6 to S8, where we see that the decrease of shunt resistance follows the experimental results very closely, while the reduction of doping in HTL or the formation of defects in the perovskite layer could also be compatible mechanisms.

These examples show how the coupling of IV and PL measurements, combined with drift diffusion simulations, provides insight into the degradation of perovskite solar cells. The formation of shunts appears to be a plausible mechanism for the samples investigated here, all fabricated with similar architectures and aged under the same damp-heat conditions.

5 Conclusion

We have developed a tool to carry out simultaneous in-situ monitoring of the dark/illuminated current-voltage characteristics and photoluminescence emission spectrum of a solar cell subjected to accelerated aging in a climate chamber. This tool was used to characterize the aging of perovskite solar cells in damp heat conditions. Using this method, a significant decoupling of the evolution of optical and electrical parameters was observed, demonstrating the complementarity of the two techniques and the major interest of this work. Two approaches are employed to investigate the underlying causes of degradation. First, the dark IV curves are fitted using a three-diode model (for the first time to our knowledge for perovskite analysis), and then the illuminated IV curves and PL spectra are studied via an original coupled optical and electrical modeling. Both approaches provide coherent insight into the source of the performance losses, pointing to the formation of shunts and the probable degradation of the top layer of the samples. Intended as a proof of principle, this study can be applied for any kind of architecture and also serve as a starting point for more in-depth in situ characterization, notably by implementing time-resolved, morphological, and chemical surface analysis techniques. Finally, the increasing number of candidate materials used in an increasing number of architectures, as well as the expansion of application areas (agriPV, floating PV, etc.), each of which requires several specific aging tests, highlight the power and usefulness of our experimental set-up for detecting the origins of degradation.

6 Authors contributions

All the authors were involved in the preparation of the manuscript. All the authors have read and approved the final manuscript.

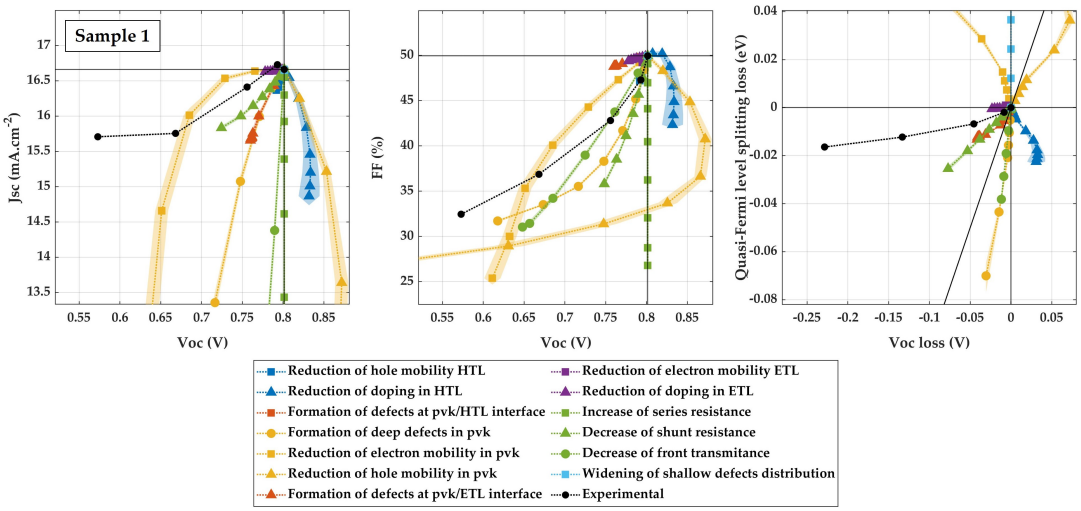

Fig. 7. Experimental and simulated degradation pathways for sample 1. A formation of shunts (green triangles) is compatible with experimental results, as it follows closely the same pathway on all planes. A formation of defects at the ETL-perovskite interface (red triangles) is also compatible with the beginning of the degradation

The authors acknowledge the IPVF fabrication team, and especially Marion Provost, for providing the samples and Karim Medjoubi for their encapsulation. This research was funded by the Agence Nationale de la Recherche under the France 2030 programme, MINOTAURE project, Grant ANR-22-PETA-0015.

References

1. M. A. Green, E. D. Dunlop, M. Yoshita, N. Kopidakis, K. Bothe, G. Siefer, D. Hinken, M. Rauer, J. Hohl-Ebinger, and X. Hao, "Solar cell efficiency tables (Version 64)," *Progress in Photovoltaics: Research and Applications*, vol. 32, no. 7, pp. 425–441, 2024. _eprint: https://onlinelibrary.wiley.com/doi/pdf/10.1002/pip.3831.
2. R. Sharma, A. Sharma, S. Agarwal, and M. S. Dhaka, "Stability and efficiency issues, solutions and advancements in perovskite solar cells: A review," *Solar Energy*, vol. 244, pp. 516–535, Sept. 2022.
3. Z. Song, N. Shrestha, S. C. Watthage, G. K. Liyanage, Z. S. Almutawah, R. H. Ahangharnejhad, A. B. Phillips, R. J. Ellingson, and M. J. Heben, "Impact of Moisture on Photoexcited Charge Carrier Dynamics in Methylammonium Lead Halide Perovskites," *J. Phys. Chem. Lett.*, vol. 9, pp. 6312–6320, Nov. 2018. Publisher: American Chemical Society.
4. A. D. Wright, J. B. Patel, M. B. Johnston, and L. M. Herz, "Temperature-Dependent Reversal of Phase Segregation in Mixed-Halide Perovskites," *Advanced Materials*, vol. 35, no. 19, p. 2210834, 2023. _eprint: https://onlinelibrary.wiley.com/doi/pdf/10.1002/adma.202210834.
5. C. C. Boyd, R. Cheacharoen, T. Leijtens, and M. D. McGehee, "Understanding degradation mechanisms and improving stability of perovskite photovoltaics," *Chemical reviews*, vol. 119, no. 5, pp. 3418–3451, 2018.
6. K. M. Fransishyn, S. Kundu, and T. L. Kelly, "Elucidating the Failure Mechanisms of Perovskite Solar Cells in Humid Environments Using In Situ Grazing-Incidence Wide-Angle X-ray Scattering," *ACS Energy Lett.*, vol. 3, pp. 2127–2133, Sept. 2018. Publisher: American Chemical Society.
7. M. V. Khenkin, E. A. Katz, A. Abate, G. Bardizza, J. J. Berry, C. Brabec, F. Brunetti, V. Bulović, Q. Burlingame, A. Di Carlo, R. Cheacharoen, Y.-B. Cheng, A. Colsmann, S. Cros, K. Domanski, M. Dusza, C. J. Fell, S. R. Forrest, Y. Galagan, D. Di Girolamo, M. Grätzel, A. Hagfeldt, E. Von Hauff, H. Hoppe, J. Kettle, H. Köbler, M. S. Leite, S. Liu, Y.-L. Loo, J. M. Luther, C.-Q. Ma, M. Madsen, M. Manceau, M. Matheron, M. McGehee, R. Meitzner, M. K. Nazeeruddin, A. F. Nogueira, C. Odabasi, A. Osherov, N.-G. Park, M. O. Reese, F. De Rossi, M. Saliba, U. S. Schubert, H. J. Snaith, S. D. Stranks, W. Tress, P. A. Troshin, V. Turkovic, S. Veenstra, I. Visoly-Fisher, A. Walsh, T. Watson, H. Xie, R. Yıldırım, S. M. Zakeeruddin, K. Zhu, and M. Lira-Cantu, "Consensus statement for stability assessment and reporting for perovskite photovoltaics based on ISOS procedures," *Nature Energy*, vol. 5, pp. 35–49, Jan. 2020.
8. X. Zhao, T. Liu, Q. C. Burlingame, T. Liu, R. Holley, G. Cheng, N. Yao, F. Gao, and Y.-L. Loo, "Accelerated aging of all-inorganic, interface-stabilized perovskite solar cells," *Science*, vol. 377, pp. 307–310, July 2022. Publisher: American Association for the Advancement of Science.
9. D. A. Chalkias, A. Karavioti, G. C. Papanicolaou, and E. Stathatos, "Stability assessment of carbon-based hole-transport-layer-free perovskite solar cells under accelerated ageing: A combined experimental and predictive modelling analysis," *Electrochimica Acta*, vol. 427, p. 140905, Sept. 2022.
10. Y. Zhao, W. Zhou, Z. Han, D. Yu, and Q. Zhao, "Effects of ion migration and improvement strategies for the operational stability of perovskite solar cells," *Physical Chemistry Chemical Physics*, vol. 23, no. 1, pp. 94–106, 2021.
11. K. Zhao, Q. Liu, L. Yao, C. Değer, J. Shen, X. Zhang, P. Shi, Y. Tian, Y. Luo, J. Xu, J. Zhou, D. Jin, S. Wang, W. Fan, S. Zhang, S. Chu, X. Wang, L. Tian, R. Liu, L. Zhang, I. Yavuz, H.-f. Wang, D. Yang, R. Wang, and

J. Xue, "peri-Fused polyaromatic molecular contacts for perovskite solar cells," *Nature*, vol. 632, pp. 301–306, Aug. 2024. Publisher: Nature Publishing Group.

12. S. Tan, T. Huang, I. Yavuz, R. Wang, T. W. Yoon, M. Xu, Q. Xing, K. Park, D.-K. Lee, C.-H. Chen, R. Zheng, T. Yoon, Y. Zhao, H.-C. Wang, D. Meng, J. Xue, Y. J. Song, X. Pan, N.-G. Park, J.-W. Lee, and Y. Yang, "Stability-limiting heterointerfaces of perovskite photovoltaics," *Nature*, vol. 605, pp. 268–273, May 2022. Publisher: Nature Publishing Group.
13. P. Chen, Y. Xiao, J. Hu, S. Li, D. Luo, R. Su, P. Caprioglio, P. Kaienburg, X. Jia, N. Chen, J. Wu, Y. Sui, P. Tang, H. Yan, T. Huang, M. Yu, Q. Li, L. Zhao, C.-H. Hou, Y.-W. You, J.-J. Shyue, D. Wang, X. Li, Q. Zhao, Q. Gong, Z.-H. Lu, H. J. Snaith, and R. Zhu, "Multifunctional ytterbium oxide buffer for perovskite solar cells," *Nature*, vol. 625, pp. 516–522, Jan. 2024. Publisher: Nature Publishing Group.
14. B. He, C. Wang, J. Li, Z. Su, G. Xing, X. Gao, and S. Chen, "In Situ and Operando Characterization Techniques in Stability Study of Perovskite-Based Devices," *Nanomaterials*, vol. 13, p. 1983, Jan. 2023. Number: 13 Publisher: Multidisciplinary Digital Publishing Institute.
15. R. Szostak, A. de Souza Gonçalves, J. N. de Freitas, P. E. Marchezi, F. L. de Araujo, H. C. N. Tolentino, M. F. Toney, F. das Chagas Marques, and A. F. Nogueira, "In Situ and Operando Characterizations of Metal Halide Perovskite and Solar Cells: Insights from Lab-Sized Devices to Upscaling Processes," *Chem. Rev.*, vol. 123, pp. 3160–3236, Mar. 2023. Publisher: American Chemical Society.
16. A. Julien, J.-B. Puel, and J.-F. Guillemoles, "Distinction of mechanisms causing experimental degradation of perovskite solar cells by simulating associated pathways," *Energy & Environmental Science*, vol. 16, no. 1, pp. 190–200, 2023. Publisher: Royal Society of Chemistry.
17. Z. Purohit, W. Song, J. Carolus, H. Chaliyawala, S. Lammar, T. Merckx, T. Aernouts, B. Tripathi, and M. Daenen, "Impact of Potential-Induced Degradation on Different Architecture-Based Perovskite Solar Cells," *Solar RRL*, vol. 5, no. 9, p. 2100349, 2021. _eprint: https://onlinelibrary.wiley.com/doi/pdf/10.1002/solr.202100349.
18. E. T. Hoke, D. J. Slotcavage, E. R. Dohner, A. R. Bowring, H. I. Karunadasa, and M. D. McGehee, "Reversible photo-induced trap formation in mixed-halide hybrid perovskites for photovoltaics," *Chem. Sci.*, vol. 6, pp. 613–617, Dec. 2014. Publisher: The Royal Society of Chemistry.
19. J. M. Howard, E. M. Tennyson, S. Barik, R. Szostak, E. Waks, M. F. Toney, A. F. Nogueira, B. R. A. Neves, and M. S. Leite, "Humidity-Induced Photoluminescence Hysteresis in Variable Cs/Br Ratio Hybrid Perovskites," *J. Phys. Chem. Lett.*, vol. 9, pp. 3463–3469, June 2018. Publisher: American Chemical Society.
20. S. Wieghold, A. S. Bieber, M. Mardani, T. Siegrist, and L. Nienhaus, "Understanding the effect of light and temperature on the optical properties and stability of mixed-ion halide perovskites," *J. Mater. Chem. C*, vol. 8, pp. 9714–9723, July 2020. Publisher: The Royal Society of Chemistry.
21. T. Vincent, D. Coutancier, P. Dally, M. Al Katrib, M. Frégnaux, S. Cacovich, F. Donsanti, A. Yaïche, K. Medjoubi, T. Guillemot, M. Provost, J. Rousset, M. Bouttemy, and N. Schneider, "Fine tuning of Nb-incorporated TiO2 thin films by atomic layer deposition and application as efficient electron transport layer in perovskite solar cells," *Journal of Vacuum Science & Technology A*, vol. 42, p. 032802, May 2024.
22. G. D. Gesesse, D. Coutancier, M. A. Katrib, F. Donsanti, M. Bouttemy, and N. Schneider, "Doped SnO $_2$ thin films fabricated at low temperature by atomic layer deposition with a precise incorporation of niobium atoms," *Nanotechnology*, vol. 35, p. 385706, Sept. 2024.
23. J. J. Yoo, G. Seo, M. R. Chua, T. G. Park, Y. Lu, F. Rotermund, Y.-K. Kim, C. S. Moon, N. J. Jeon, J.-P. Correa-Baena, V. Bulović, S. S. Shin, M. G. Bawendi, and J. Seo, "Efficient perovskite solar cells via improved carrier management," *Nature*, vol. 590, pp. 587–593, Feb. 2021.
24. P. Würfel, S. Finkbeiner, and E. Daub, "Generalized Planck's radiation law for luminescence via indirect transitions," *Appl. Phys. A*, vol. 60, pp. 67–70, Jan. 1995.
25. J. K. Katahara and H. W. Hillhouse, "Quasi-Fermi level splitting and sub-bandgap absorptivity from semiconductor photoluminescence," *Journal of Applied Physics*, vol. 116, p. 173504, Nov. 2014.
26. M. Burgelman, P. Nollet, and S. Degrave, "Modelling polycrystalline semiconductor solar cells," *Thin solid films*, vol. 361, pp. 527–532, 2000.
27. S. Suckow, "2/3-Diode Fit, available on https://nanohub.org/resources/14300," 2014.
28. F. Hernando, R. Gutierrez, G. Bueno, F. Recart, and V. Rodriguez, "Humps, a surface damage explanation," *Proceedings of 2nd. World Conference and Exhibition on Photovoltaic Solar Energy Conversion*, pp. 1321–1323, 1998.
29. K. McIntosh, "Phd thesis. lumps, humps and bumps : three detrimental effects in the current-voltage curve of silicon solar cells," 2001.
30. O. Breitenstein, P. Altermatt, K. Ramspeck, and A. Schenk, "The Origin of Ideality factors n > 2 of Shunts and Surfaces in the Dark I-V Curves of Si Solar Cells," (Dresden), 2006.
31. R. Scheer and H. Schock, *Chalcogenide Photovoltaics: Physics, Technologies, and Thin Film Devices*. Wiley, 1 ed., Feb. 2011.
32. N. Courtier, "Interpreting ideality factors for planar perovskite solar cells: Ectypal diode theory for steady-state operation," *Physical Review Applied*, vol. 14, no. 2, p. 024031, 2020.
33. W. Tress, M. Yavari, K. Domanski, P. Yadav, B. Niesen, J. P. C. Baena, A. Hagfeldt, and M. Graetzel, "Interpretation and evolution of open-circuit voltage, recombination, ideality factor and subgap defect states during reversible light-soaking and irreversible degradation of perovskite solar cells," *Energy and Environmental Science*, vol. 11, pp. 151–165, 2018.
34. T. Campos, P. Dally, S. Gbegnon, A. Blaizot, G. Trippé-Allard, M. Provost, M. Bouttemy, A. Duchatelet, D. Garrot, J. Rousset, and E. Deleporte, "Unraveling the Formation Mechanism of the 2D/3D Perovskite Heterostructure for Perovskite Solar Cells Using Multi-Method Characterization," *The Journal of Physical Chemistry C*, vol. 126, pp. 13527–13538, Aug. 2022.